AIAA JOURNAL
Vol. 34, No. 3, March 1996

Influence of Surface Flow on Aerodynamic Loads of a Cantilever Wing

Rong F. Huang,* Wen W. Shy,† and Song W. Lin†
National Taiwan Institute of Technology, Taipei, Taiwan, Republic of China
and
Fei-Bin Hsiao‡
National Cheng Kung University, Tainan, Taiwan, Republic of China

The properties of the characteristic surface flow modes and their influence on the aerodynamic loads of a cantilever wing at low chord Reynolds numbers were experimentally studied. The chordwise variations of the separation and reattachment locations as well as the length and center position of the separation bubble in the domain of the chord Reynolds number/root angle of attack heavily depend on the characteristic surface flow modes. The aerodynamic loads, e.g., the lift, drag, and moment coefficients, are profoundly influenced by the characteristic behaviors of suction surface flow. The lift coefficient increases with the increase of root angle of attack in the regimes of laminar separation, separation bubble, and transition. The curve of lift coefficient has a largest slope in the laminar separation regime. The increase rate of the lift coefficient decreases when the separation bubble is formed. The stall happens in the turbulent separation regime. The drag coefficient slightly decreases in the laminar separation regime, remains almost a constant in the separation bubble regime, and increases in the transition regime.

Nomenclature

b	= span of wing, 30 cm
C	= chord length of wing, 6 cm
C_D	= drag coefficient, D/qbC
C_L	= lift coefficient, L/qbC
C_M	= moment coefficient of pitching about quarter chord, M/qbC^2
D	= drag force, measured by balance in freestream direction
f	= frequency
L	= lift force, measured by balance in cross freestream direction
M	= pitching moment about quarter-chord location
q	= dynamic pressure of freestream, $\frac{1}{2}\rho_w u_w^2$
Re_c	= Reynolds number based on chord length of wing
t	= time
u_w	= freestream velocity in wind-tunnel test section
X	= streamwise coordinate, originated from leading edge of wing on root-plane
X_r	= streamwise position of reattachment point of separated boundary layer on suction side surface of wing
X_s	= streamwise position of separation point of boundary layer on suction side surface of wing
Y	= spanwise coordinate, originated from leading edge of wing on root-plane
Z	= cross stream coordinate, originated from leading edge of wing on root-plane
α_0	= root angle of attack
ΔX_b	= chordwise length of separation bubble
ρ_w	= density of free airstream in wind-tunnel test section
ϕ	= power spectrum of freestream velocity

Received April 13, 1995; revision received Oct. 18, 1995; accepted for publication Oct. 28, 1995.

*Associate Professor, Department of Mechanical Engineering, 43 Keelung Road, Sec. 4. Member AIAA.
†Graduate Student, Department of Mechanical Engineering, 43 Keelung Road, Sec. 4.
‡Professor, Institute of Aeronautics and Astronautics. Member AIAA.

Introduction

THE characteristics of the flow over a two-dimensional wing at low Reynolds numbers have been studied by many investigators. Most of the studies were focused on the behavior of the surface flows on the suction surface, e.g., laminar separation, transition, reattachment, etc., because of its significant influence on the aerodynamic performance.[1–5] The general behavior of the surface flows on the low Reynolds number wings has been described by Lissaman in his excellent review paper.[6] The laminar boundary layer, extending from the stagnation point over the leading edge, separates downstream of the point of minimum pressure under certain flow condition and wing configuration. Transition to turbulent flow occurs in the free shear layer a short distance downstream from the separation point. The flow then reattaches to the wing surface, with a turbulent boundary layer extending from the reattachment point to the trailing edge. A recirculation bubble is found between the separation and reattachment points once the boundary layer reattaches. At low chord Reynolds numbers and angles of attack, the bubble generally extends a large portion of the chord length and significantly changes the pressure distribution by effectively altering the shape over which the outer potential stream flows. The separation bubble can hence significantly change the aerodynamic performance.[7]

The systematic survey of the surface flow patterns of a NACA 0012 cantilever wing at the very low end of Reynolds numbers has recently been reported.[8] The characteristic domain of their results is reproduced in Fig. 1. Three characteristic surface flow modes—attached boundary layer (region A), laminar separation (region B), and complete separation (region C)—for chord Reynolds number lower than 2.2×10^4 and five characteristic surface flow modes—laminar separation (region D), separation bubble (region E), transition (region F), turbulent separation (region G), and three-dimensional flow (region H)—for chord Reynolds number between 3.8×10^4 and 1.2×10^5 were identified in the domain of chord Reynolds number/root angle of attack, as shown in Fig. 1. Within the range of experiment, the three-dimensional effects of the wall and wing tip on the flow patterns are not significant for $Y/C > 0.5$ and < 4.6, respectively. These characteristic flow modes are classified according to the smoke streaks or surface oil-flow patterns observed in the range between $Y/C \approx 0.6$ and 4.5. For flows in region A, the attached boundary-layer regime, the laminar boundary layers on the suction and pressure sides of the wing, are all attached to the surfaces. For flows in region B, the laminar separation

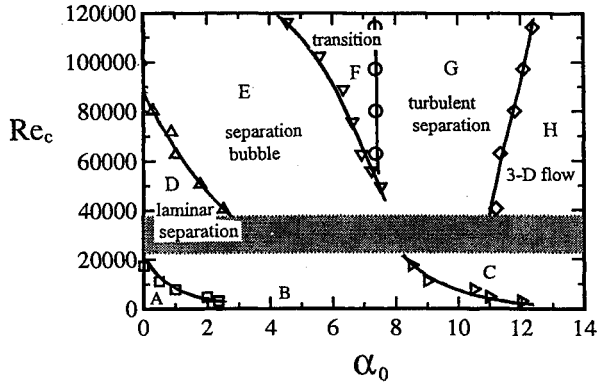

Fig. 1 Regions of characteristic flow modes in domain of chord Reynolds number/root angle of attack. Reproduced from Huang and Lin.[8]

regime, the laminar boundary layer on the suction surface, separates. In region C, the complete separation regime, the boundary layer separates almost from the leading edge. The reattachment of the separated boundary layer is not found in these very low Reynolds number regimes A, B, and C. For chord Reynolds number between 3.8×10^4 and 2.2×10^5, the behavior of the surface flow becomes more complicated. In region D, the location of separation moves toward the leading edge with the increase of root angle of attack or Reynolds number. In region E, the separation bubble regime, the separated surface reattaches to form a separation bubble. The bubble moves toward the leading edge and becomes smaller with the increase of root angle of attack. However, the separation location moves downstream with the increase of chord Reynolds number. In region F, the transition regime, the boundary layer is in transition from a laminar to a turbulent state. Both separation and reattaching lines move upstream with the increase of root angle of attack. In region G, the turbulent separation regime, the turbulent boundary layer separates in the downstream area of a short leading-edge separation bubble. The separation line stays very close to the leading edge and does not appreciably move with the increase of root angle of attack. In region H, the three-dimensional flow regime, strong three-dimensional flow pattern is observed. Two surface vortices, one near the root area and the other near the wing tip, are generated because of the strong wall and end effects.

These characteristic surface flow modes were found to be closely related to the complex behavior of the vortex shedding in the wake region.[8] However, the properties of these characteristic flow modes and their influence on the aerodynamic performance were still not reported yet. Beacuse of the variation of the surface flow modes at low Reynolds numbers, the aerodynamic performance of a cantilever wing may exhibit complex behavior. In this paper, we present the experimental results showing the properties of the characteristic surface flow modes and their influence on the aerodynamic loads of a cantilever wing at low Reynolds numbers.

Experimental Setup

The experiments were performed in an open-loop wind tunnel, as shown in Fig. 2. The test section size was $60 \times 60 \times 120$ cm. The maximum turbulence intensity is less than 0.2% within the operating range of 0.5–52 m/s. Figures 3a–3c show the typical instantaneous velocity, probability density function (pdf), and power spectrum, respectively, of the freestream at $u_w = 23.63$ m/s. The instantaneous velocity data shown in Fig. 3a were taken with a hot-wire anemometer at a rate of 12,000 samples/s. The turbulence intensity is 0.11%. The probability density function of the randomly fluctuating velocity almost follows the Gaussian distribution with standard deviation 0.025 m/s, as shown in Fig. 3b. The power spectrum in Fig. 3c shows no special peak. The broadband extends up to about 2000 Hz and then decays. The nonuniformity of the average velocity profile across the cross-section is lower than 0.5%. During the experiments the velocity of the approaching flow was monitored with a pitot-static tube. An aluminum plate with sharp leading and trailing edges was placed 5 cm above the floor of the test section for control of the boundary-layer thickness.

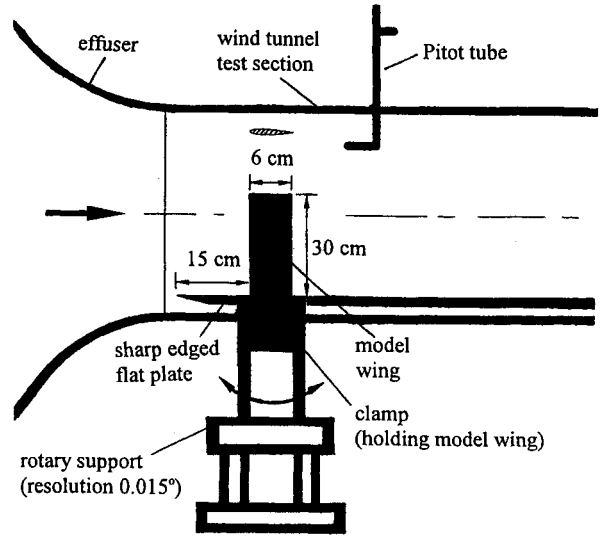

Fig. 2 Experimental setup.

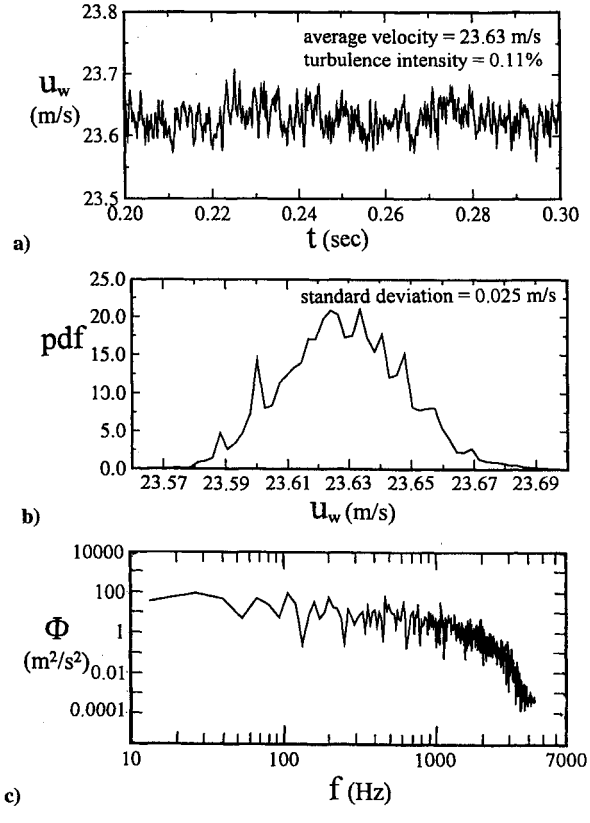

Fig. 3 Typical statistical information of freestream velocity in wind-tunnel test section measured by a hot-wire anemometer at $u_w = 23.63 \pm 0.35$ m/s: a) instantaneous velocity, b) probability density function, and c) power spectrum.

The rectangular wing model is made of aluminum. The profile of the cross-section is NACA 0012. The wing tip is sharp edged. A chord length of 6 cm and span of 30 cm gives an aspect ratio of 5. The wing model is mounted on a JR^3 Universal Force-Moment System, which is in turn mounted on a rotary support. The JR^3 balance has a monolithic six-degree-of-freedom force sensor. The capability of maximum dynamic response is estimated to be about 250 Hz. The wing model protrudes perpendicularly through the aluminum floor of the test section and the boundary-layer thickness control plates. The positions of separation and reattachment of the boundary layer on the suction surface of the wing were taken from the recorded images of the smoke streaks and surface oil-flow patterns.[8]

The accuracy of the freestream velocity measurement is primarily affected by the alignment of the pitot tube and the calibration of

the pressure transducer. With the help of an on-line micropressure calibration system and careful alignment of the pitot tube, the uncertainty of the freestream velocity was estimated to be as large as 3%. The rotary support has a resolution of 0.015 deg. The accuracy of the root angle of attack was controlled within 0.5%. The uncertainty in separation location is estimated to be less than 3%. The uncertainty in reattachment location is less than 5%. The accuracy of the force-moment measurement is affected by the mounting of the wing and the calibration of the balance. With the help of a specially designed mounting block and a calibration matrix, the uncertainties of lift and drag are estimated to be as large as 5 and 8%, respectively. The uncertainty of moment data are less than 7%.

Results and Discussion

Separation and Reattachment Characteristics

In the laminar separation and separation bubble regimes (regions B, D, and E of Fig. 1), the chordwise location of the separation point in the central region varies with chord Reynolds number and root angle of attack. Figures 4a and 4b show the variation of X_s/C with α_0 at $Y/C = 3$ in the laminar separation (region B) and separation bubble (region E) regimes. Within the range of experiment the flow is basically two dimensional for $0.5 < Y/C < 4.6$ (Ref. 8). The locations of measurements of X_s/C are in the two-dimensional region. In both Figs. 4a and 4b, the chordwise location of the separation point moves upstream with the increase of root angle of attack until reaching the leading edge. The forward movement of separation with increasing root angle of attack is due primarily to the more severe adverse pressure gradient occurring at higher incidence. For separation without reattachment (regions B and D), the separation point moves upstream with the increase of the chord Reynolds number. However, as the separated boundary layer reattaches to the suction surface (region E) or as the separation bubble is formed, the separation point moves downstream with the increase of chord Reynolds number. This characteristic can be clearly seen from Figs. 5a and 5b. The adverse pressure gradient increases with the increase of Reynolds number when the boundary layer is not reattached to form the bubble. As the reattachment occurs, the bubble height decreases with the increase of the Reynolds number because the momentum increases, as indicated by Hsiao et al.[5] The outer inviscid flow also reduces its deflection from the wing surface with the decrease of the bubble height. The decreased deflection of the outer inviscid flow relieves the adverse pressure gradient. The separation point hence moves

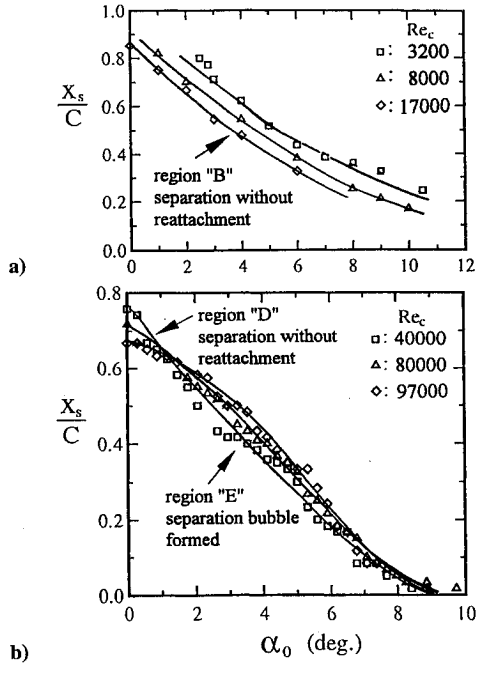

Fig. 4 Variation of chordwise location of boundary-layer separation with root angle of attack. Uncertainty in $X_s/C = \pm 1.5\%$.

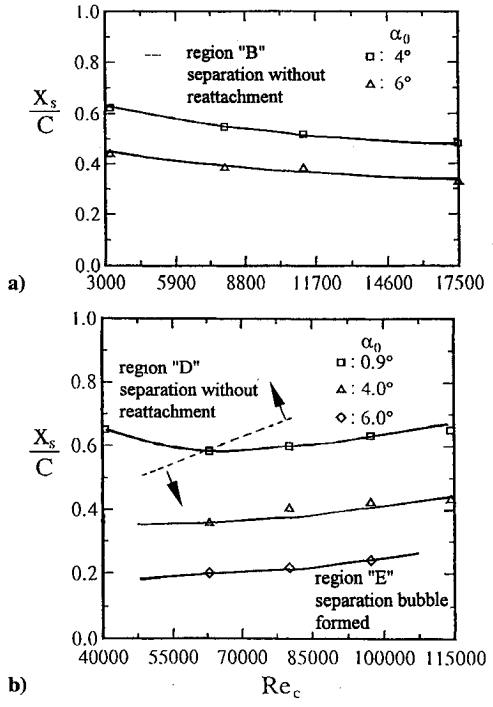

Fig. 5 Variation of chordwise location of boundary-layer separation with chord Reynolds number. Uncertainty in $X_s/C = \pm 1.5\%$.

downstream with the increase of Reynolds number as the bubble is formed.

At low chord Reynolds numbers, the separated boundary layer does not reattach to the suction surface, whereas for chord Reynolds number higher than 3.8×10^4 the reattachment is observed. The variations of the chordwise location of the reattachment point at $Y/C = 3$ with the root angle of attack and chord Reynolds number are shown in Figs. 6a and 6b. The chordwise location of the reattachment point moves upstream with the increase of root angle of attack (Fig. 6a) or chord Reynolds number (Fig. 6b). The variations are all nonlinear. Figures 7a and 7b show the variations of the separation bubble with root angle of attack and chord Reynolds number. The area between the two bold lines is where the separation bubble stays. The dashed line represents the chordwise location of the center of the separation bubble. The center of the bubble moves upstream with the increase of root angle of attack, as shown in Figs. 7a–7c. The motion of the bubble is very sensitive to the variation of the root angle of attack. The center of the separation bubble moves slightly, although not significantly, upstream with the increase of chord Reynolds number as shown in Figs. 7d–7f. The decrease of X_r/C and increase of X_s/C with Re_c cause the slight variation of the chordwise location of the bubble center. The chordwise size of the separation bubble shrinks with the root angle of attack and chord Reynolds number, as shown in Figs. 8a and 8b. The separation bubble may occupy approximately up to 45% of the chord length at low Reynolds number of 4×10^4 and root angle of attack of 2.7 deg. This large portion of coverage may significantly alter the characteristics of the aerodynamic performance, according to Lissaman.[6]

Influence of Surface Flow on Aerodynamic Loads

The aerodynamic performance of a wing is profoundly influenced by the behavior of the boundary layer on the suction side surface and the three-dimensional effects of wall and tip. Since the surface area influenced by the wall and tip effects is much less than 20% in most experiments of this study, this paper focuses on the effects of the two-dimensional behavior of the surface flow on the aerodynamic loads.

Figures 9a and 9b show the variation of the lift coefficient C_L with root angle of attack at chord Reynolds numbers of 7.6×10^4 and 1×10^5, respectively. The value of the lift coefficient increases monotonically with the increase of root angle of attack when the surface flow on the suction side surface is in the regime of laminar

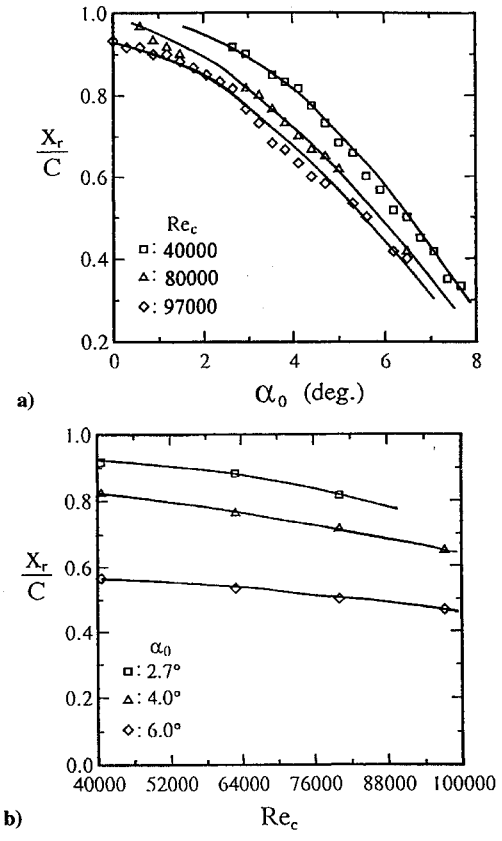

Fig. 6 Variation of chordwise location of reattachment with a) root angle of attack and b) chord Reynolds number. Uncertainty in $X_s/C = \pm 2.5\%$.

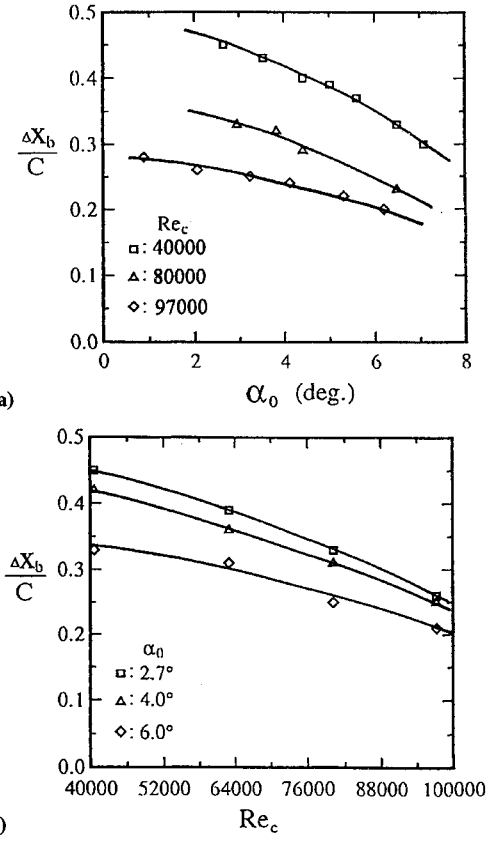

Fig. 8 Variation of chordwise bubble length with a) root angle of attack and b) chord Reynolds number. Uncertainty in $\Delta X_b/C = \pm 4\%$.

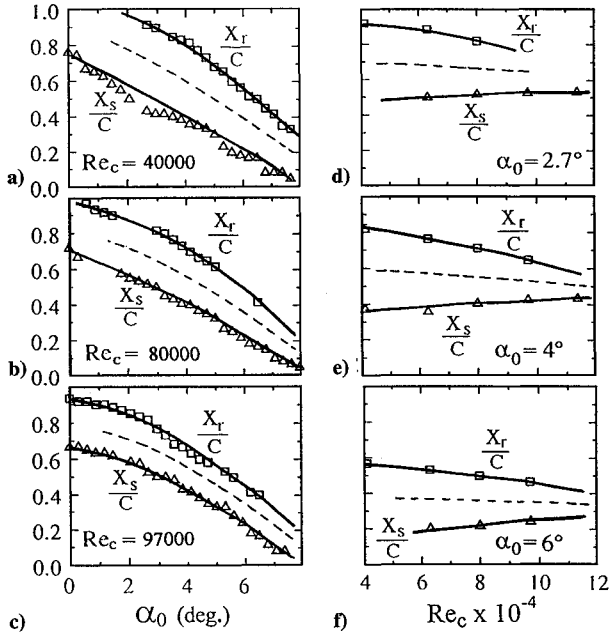

Fig. 7 Separation bubble characteristics. Uncertainties in $X_s/C = \pm 1.5\%$ and $\pm 2.5\%$.

separation, separation bubble, or transition. In the laminar separation regime, the value of the lift coefficient increases almost linearly with root angle of attack. The increase rate, $\Delta C_L/\Delta\alpha_0$, is about $(2.22 \pm 0.06)\pi$/rad for $Re_c = 7.6 \times 10^4$ and $(2.45 \pm 0.07)\pi$/rad for $Re_c = 1 \times 10^5$. The theoretical value obtained from the analytical analysis of a two-dimensional thin, symmetric flat-plate airfoil in inviscid flow is 2π/rad.[9] Abbott and van Doenhoff[10] indicated that, for wing sections approximately 12% thick, the lift-curve slope is about 9% greater than its limiting value for thin sections. Hence, the theoretical slope of the lift curve of a 12% thick wing section in inviscid flow should be about 2.18π/rad. The slope of the lift curve in the laminar separation regime of the cantilever wing is slightly greater than the theoretical value of the wing section in inviscid flow. The viscous and three-dimensional effects may be the reasons causing this deviation. In the separation bubble regime the slope of the $C_L - \alpha_0$ curve becomes noticeably smaller than that in the laminar separation regime. The slope of the lift curve in the separation bubble regime is about $(1.27 \pm 0.03)\pi$/rad for $Re_c = 7.6 \times 10^4$ and $(1.28 \pm 0.03)\pi$/rad for $Re_c = 1 \times 10^5$. The formation of the separation bubble has a negative effect on the lift of the wing. The curve seems not to follow a linear relationship at Reynolds number of 7.6×10^4. It becomes, however, almost linear at Reynolds number of 1×10^5. In the transition regime, the slope of the $C_L - \alpha_0$ curve further decreases to $(0.89 \pm 0.02)\pi$/rad for $Re_c = 7.6 \times 10^4$ and $(1.08 \pm 0.03)\pi$/rad for $Re_c = 1 \times 10^5$. The maximum value of C_L is about 0.80 ± 0.02 for $Re_c = 7.6 \times 10^4$ and 0.84 ± 0.02 for $Re_c = 1 \times 10^5$. The maximum value increases with the increase of Reynolds number. According to Abbott and van Doenhoff,[10] however, the maximum value of lift coefficient of a NACA 0012 wing section remains at a constant of about 1.60 and the slope of the lift curve is independent of Reynolds number. The lift begins to decrease when the surface flow is in the turbulent separation regime. In the turbulent separation regime, the reattached turbulent surface flow separates again to form a second separation. The second separation line moves toward the leading edge with the increase of root angle of attack. With the forward motion of the second separation line, the wing goes into the stall regime. The minimum C_L value at deep stall is about 0.59 ± 0.01 for $Re_c = 7.6 \times 10^4$ and 0.64 ± 0.02 for $Re_c = 1 \times 10^5$. The lift increases again as the root angle of attack is further increased to the three-dimensional flow regime.

Figures 10a and 10b show the variation of the drag coefficient C_D with root angle of attack at chord Reynolds numbers of 7.6×10^4 and 1×10^5, respectively. In the laminar separation regime, the drag slightly decreases with the increase of root angle of attack. The percentage of the area covered by the reverse flow because of the

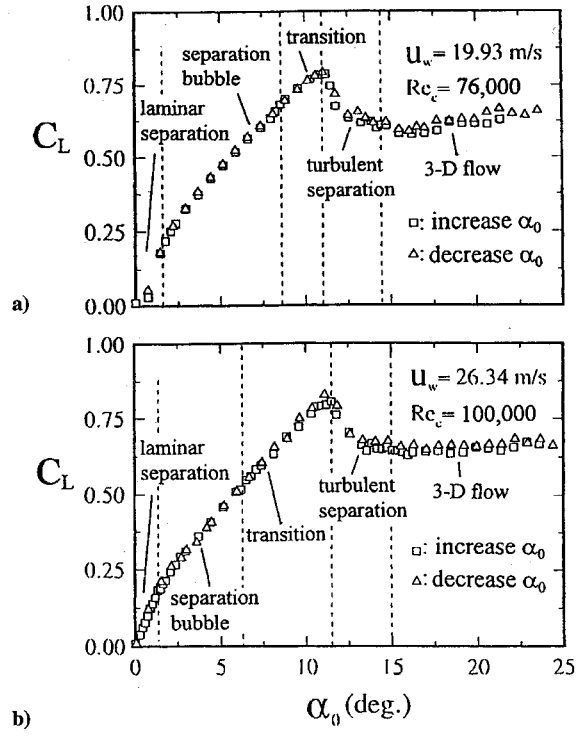

Fig. 9 Variation of lift coefficient with root angle of attack: a) Re_c = 7.6 × 10^4 and b) Re_c = 1 × 10^5. Uncertainty in C_L = ±2.5%.

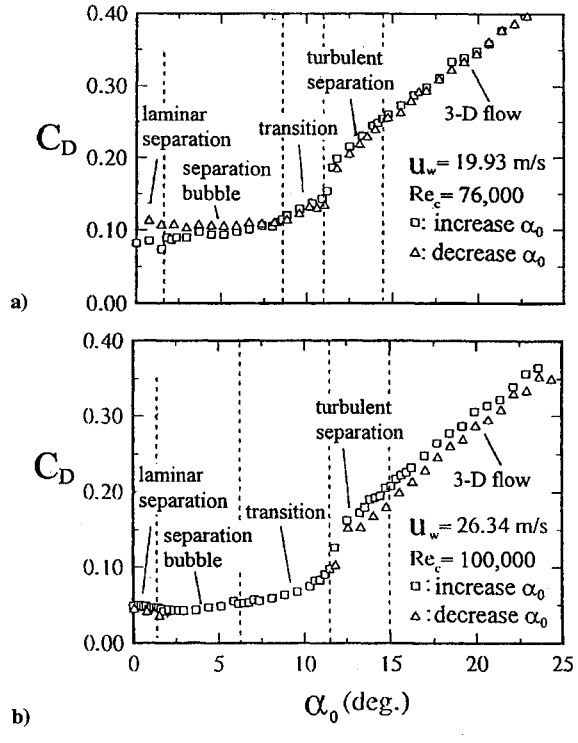

Fig. 10 Variation of drag coefficient with root angle of attack: a) Re_c = 7.6 × 10^4 and b) Re_c = 1 × 10^5. Uncertainty in C_D = ±4%.

laminar separation on the suction surface increases with the increase of the root angle of attack. The reverse flow on the suction surface contributes a reverse shear in the $-X$ direction. The increase of the reverse shear slightly decreases the drag in the laminar separation regime. In this regime, the value of C_D is about 0.10 ± 0.01 for Re_c = 7.6 × 10^4 and 0.05 ± 0.004 for Re_c = 1 × 10^5. The low C_D value at high Reynolds number in this regime is caused by the high coverage ratio of the reverse flow at high Reynolds numbers. In the separation bubble regime, the bubble moves toward the leading edge and reduces its size with the increase of the root angle of attack. The reduction of the reverse shear decreases the shear drag

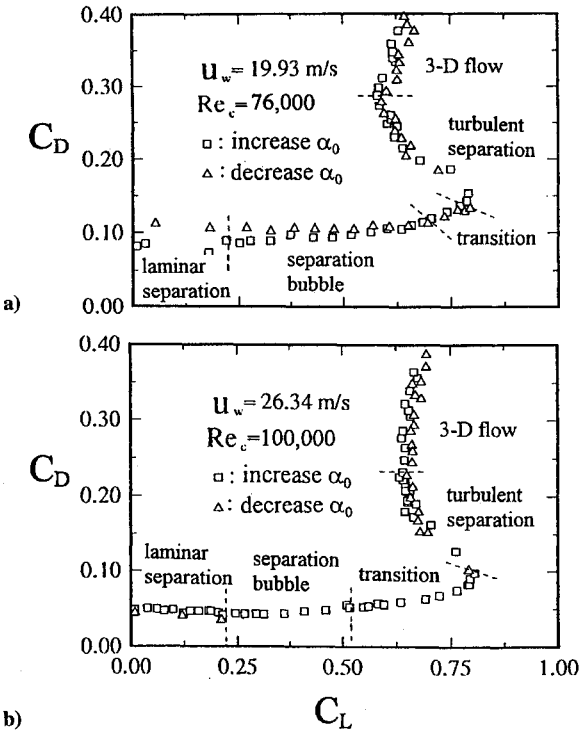

Fig. 11 Variation of drag coefficient with lift coefficient: a) Re_c = 7.6 × 10^4 and b) Re_c = 1 × 10^5. Uncertainties in C_L = ±2.5% and C_D = ±4%.

and compensates the increase of the form drag. The drag coefficient hence does not vary much in the separation bubble regime. In the transition regime, the increase of skin friction and decrease of bubble size in this regime lead to the gradual increase of drag coefficient. The slope of the drag curve increases significantly when the surface flow is in the turbulent separation regime. In the turbulent separation regime, the reattached turbulent surface flow creates a large skin friction on the suction surface.[11] Accordingly, a large increase in the drag coefficient is observed in Figs. 10a and 10b. The drag coefficient increases almost linearly with the increase of the root angle of attack in the regimes of turbulent separation and three-dimensional flow. At high angles of attack as in the three-dimensional flow regime, the form drag should play a significant role; therefore, the linear increase in the drag coefficient is not unexpected.

The contour mappings of the drag coefficient with respect to the lift coefficient at chord Reynolds numbers of 7.6 × 10^4 and 1 × 10^5 are shown in Figs. 11a and 11b. The drag coefficient does not increase with the increase of the lift coefficient in the laminar separation and separation bubble regimes. The drag coefficient increases slowly with the increase of the lift coefficient when the flow goes through the transition regime. When the surface flow proceeds to the turbulent separation regime, the drag coefficient increases rapidly and the lift coefficient decreases. The critical root angle of attack is about 11.3 ± 0.06 deg. At high angles of attack as in the three-dimensional flow regime, the wing pays much for the expense of drag coefficient with only a little increase in the lift coefficient.

The aerodynamic center of a NACA 0012 wing section is located at quarter-chord. Theoretically, the quarter-chord moment coefficient of the symmetric thin wing at high Reynolds number is zero within the linear limits of the lift curve. The quarter-chord moment coefficient of the present cantilever wing at low Reynolds number varies with the root angle of attack, as shown in Figs. 12a and 12b for chord Reynolds numbers of 7.6 × 10^4 and 1 × 10^5, respectively. The curve of the quarter-chord moment coefficient changes slope in each characteristic flow regime. The moment coefficient increases almost linearly with the increase of the root angle of attack in the laminar separation regime. It decreases with the increase of root angle of attack in the separation bubble and transition regimes. The lift increases much and the drag remains almost constant in the separation bubble and transition regimes. Therefore, the pressure center, or the position applied by the resultant force of lift and drag, must move

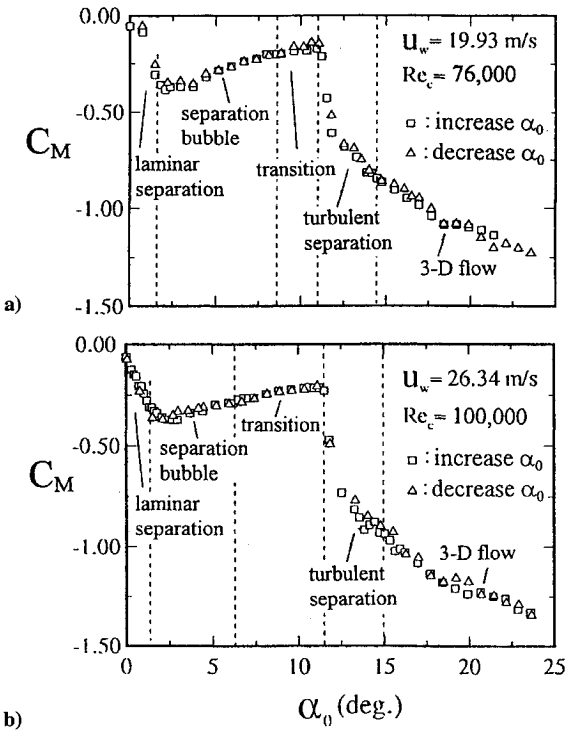

Fig. 12 Variation of moment coefficient with root angle of attack: a) $Re_c = 7.6 \times 10^4$ and b) $Re_c = 1 \times 10^5$. Uncertainty in $C_M = \pm 3.5\%$.

toward the quarter-chord with the increase of the root angle of attack when the surface flow on the suction surface proceeds in the separation bubble and transition regimes. In the turbulent separation and three-dimensional flow regimes, where the stall occurs, the lift decreases and the pressure center moves toward the trailing edge. The quarter-chord moment coefficient hence increases with root angle of attack, as has been seen in most of the performance curves of wing sections.[10]

Concluding Remarks

The chordwise variations of the separation and reattachment locations as well as the length and center position of the separation bubble in the domain of the chord Reynolds number/root angle of attack are heavily dependent on the characteristic surface flow modes. The chordwise location of the separation point moves upstream with the increase of root angle of attack until reaching the leading edge. For separation without reattachment, the separation point moves upstream with the increase of the chord Reynolds number. However, as the separated boundary layer reattaches to the suction surface, or as the separation bubble is formed, the separation point moves downstream with the increase of chord Reynolds number. The chordwise location of the reattachment point moves upstream with the increase of root angle of attack or chord Reynolds number. The center of the bubble moves upstream with the increase of root angle of attack. It moves just slightly upstream with the increase of chord Reynolds number. The chordwise size of the separation bubble shrinks with the root angle of attack and chord Reynolds number. The aerodynamic loads, e.g., the lift, drag, and moment coefficients, are profoundly influenced by the characteristic behaviors of suction surface flow. The lift coefficient increases with the increase of root angle of attack in the regimes of laminar separation, separation bubble, and transition. The lift curve has its largest slope in the laminar separation regime. The slope decreases when the separation bubble is formed. The stall happens as the surface flow proceeds to the turbulent separation regime. The drag coefficient slightly decreases in the laminar separation regime, remains almost a constant in the separation bubble regime, and increases in the transition regime. It increases to the largest degree in the turbulent separation regime.

Acknowledgment

This study was supported by the National Science Council of the Republic of China under Grant NSC 85-2212-E-011-012.

References

[1]Ward, J. R., "The Behavior and Effects of Laminar Separation Bubbles on Airfoils in Incompressible Flow," *Journal of the Royal Aeronautical Society*, Vol. 67, Dec. 1963, pp. 783–790.

[2]Arena, A. V., and Mueller, T. J., "Laminar Separation, Transition, and Turbulent Reattachment Near the Leading Edge of Airfoils," *AIAA Journal*, Vol. 18, No. 7, 1980, pp. 747–753.

[3]Pohlen, L. J., and Mueller, T. J., "Boundary Layer Characteristics of the Miley Airfoil at Low Reynolds Numbers," *Journal of Aircraft*, Vol. 21, No. 9, 1983, pp. 658–664.

[4]O'Meara, M. M., and Mueller, T. J., "Laminar Separation Bubble Characteristics on an Airfoil at Low Reynolds Numbers," *AIAA Journal*, Vol. 25, No. 8, 1987, pp. 1033–1041.

[5]Hsiao, F.-B., Liu, C.-F., and Tang, Z., "Aerodynamic Performance and Flow Structure Studies of a Low Reynolds Number Airfoil," *AIAA Journal*, Vol. 27, No. 2, 1989, pp. 129–137.

[6]Lissaman, P. B. S., "Low Reynolds Number Airfoils," *Annual Review of Fluid Mechanics*, Vol. 15, No. 2, 1983, pp. 223–239.

[7]Marchman, J. F., "Aerodynamic Testing at Low Reynolds Numbers," *Journal of Aircraft*, Vol. 24, No. 2, 1987, pp. 107–114.

[8]Huang, R. F., and Lin, C. L., "Vortex Shedding and Shear-Layer Instability of Wing at Low Reynolds Numbers," *AIAA Journal*, Vol. 33, No. 8, 1995, pp. 1398–1403.

[9]Bertin, J. J., and Smith, M. L., *Aerodynamics for Engineers*, Prentice–Hall, Englewood Cliffs, NJ, 1989, pp. 207–213.

[10]Abbott, I. H., and von Doenhoff, A. E., *Theory of Wing Section*, Dover, New York, 1959, pp. 50–53.

[11]Bertin, J. J., and Smith, M. L., *Aerodynamics for Engineers*, Prentice–Hall, Englewood Cliffs, NJ, 1989, pp. 150–156.